Naturally Inspired SERS Substrates

4

N. L. Garrett

1 Definition of Topic

This topic concerns the application of naturally occurring nanostructures to surface-enhanced Raman spectroscopy.

2 Overview

Surface-enhanced Raman scattering (SERS) is a powerful spectroscopic analytical tool with a wide range of applications. Many market sectors benefit from SERS, in fields as diverse as: clinical diagnostics, pharmaceuticals, forensics, environmental evaluation, and biochemical studies. Demand for improved sensitivity, throughput, specificity, and cost efficiency in industry constantly drives advances in assay technology. This chapter outlines the recent advances in SERS substrate production inspired by naturally occurring nanostructures and their application to the problem of detecting protein-binding events.

3 Introduction

Since the turn of the twentieth century, interesting optical effects from optically small metal interfaces and structures have been the subject of much scrutiny. Molecules adsorbed onto rough metal surfaces, particles, or island films exhibit dramatically different optical properties to those of the free molecules [1]. Perhaps

N.L. Garrett
School of Physics, University of Exeter, Devon, UK

Challa S. S. R. Kumar (ed.), *Raman Spectroscopy for Nanomaterials Characterization*,
DOI 10.1007/978-3-642-20620-7_4,

the most widely known effect of this nature is surface-enhanced Raman scattering (SERS) where the Raman signal from molecules adsorbed onto suitable metallic substrates can be millions of times stronger than that from the free molecule. The SERS effect has found wide application in biology, medicine, electrochemistry, and materials science through such techniques as SERS of single molecules, nanostructures and transition metals, tip-enhanced Raman Scattering (TERS), surface-enhanced hyper-Raman scattering (SEHRS), ultraviolet-excited SERS (UV-SERS) [2]. Other examples of such metal enhancement exist, such as surface-enhanced infrared absorption [1] and plasmon-enhanced spectroscopy [2].

Recently, several reports have demonstrated the potential of SERS as a label-free readout for monitoring protein-binding events [3–5]. The potential for low detection limits and higher sensitivities available with SERS have been exploited in recent biological assay research [6–8] but this has been limited by the irreproducible enhancement provided by the substrates available for aqueous experiments, such as colloidal metals. Due to the requirement for conjugation of colloidal metallic particles to give substantial enhancements and the change of enhancement with aggregation, colloidal-based SERS methods are not reproducible, and metallic particles are prone to settling out of suspension during scanning.

Many available SERS substrates require the analyte to be deposited and dried prior to scanning. This is unsuitable for most biological analytes, such as proteins, since the process of desiccation alters their configuration and hence their Raman spectrum [9]. Drop-coated deposition has been claimed to produce un-enhanced Raman spectra of proteins analogous to those obtained from aqueous proteins [10] by providing a "natural" environment. However, with protein structure being strongly dependent upon the hydration of the molecule, it is essential that aqueous conditions are maintained in order to perform rigorous investigation of proteins. Protein-binding systems are complex interactions which require optimal protein structure for binding to occur. Variation in pH, hydration, and temperature can profoundly alter on protein structure, thus preventing binding events which can lead to a dramatic reduction in the detection sensitivity [11].

SERS assays using proteins have traditionally required highly complex systems with multiple interactions to produce a detectable event [3, 5], usually with colloidal noble metal particles or a SERS chemical label providing the means of detecting binding events. These assays can provide high sensitivity to low levels of analyte in solution, but the interaction of metal colloids and chemical SERS marker molecules has the potential to adversely affect the biological molecules of interest. Intricate multiple-stage assays are undesirable for complex biological systems, where assays are required to be highly robust if they are to be of use. More cutting-edge assays have used dielectric-core metal-coated nanoshells bioconjugated to antibodies [5, 12–14]. These assays produce excellent sensitivity combined with low levels of undesired biological interaction between the label and the analyte. However, with the nanoshells free in solution, SERS spectra can be difficult to reproduce unless the analyte is spun down using centrifugation or immobilized in some manner; these processes can be damaging to some biological samples.

The ideal substrate for SERS would provide highly reproducible SERS enhancement factors of the order of 10^6 or higher. Other requirements include the ability to perform rapid SERS biological assays whilst the samples are hydrated, which are sensitive over a range of concentrations that are comparable with ELISA and other highly sensitive assaying techniques. A principle challenge to providing these qualities in a SERS substrate is designing a suitable nanostructure that is not prohibitively expensive to produce or use in high through-put applications. In search of less expensive methods for SERS substrate production, in recent years scientists have taken inspiration from naturally occurring nanostructures.

Scientists in a broad variety of fields exploit various forms of nanostructures inspired by nature [15]. Naturally occurring nanostructures that have evolved for functions involving visual appearance have been the subject of a remarkable surge in research interest [16–20]. This has built upon a range of somewhat earlier studies [21, 22]. Numerous insects, birds, and plants exhibit a wide array of complex periodic and quasi-periodic ultrastructure. Their nanostructures can contribute to many biological functions: highly unsaturated color appearances for short- or long-range conspecific communication [23, 24]; angle-independent color [25] and specular or diffuse broadband appearances [26] for specialized camouflaging; linearly [24] or circularly polarized reflection [27] for high-level communication, represent a few of these.

One investigation into the optical properties of cicada wings found that the "quasiperiodic" nanostructured antireflective coating on the chitinous wing surfaces provided an excellent SERS substrate, with enhancement factors of approximately 10^6 [28]. These structures have been reproduced using a biotemplating approach for silver-coated nanoimprinted optical fibers in SERS sensing [29]. The imprinting procedure involved producing heat-cured elastomer casts of cicada wing segments, imprints of which were formed on wet polymer in contact with glass fibers under a three-step curing procedure. Although the silver-coated substrates in this study were found to be robust and inexpensive, the SERS spectra from thiophenol monolayers deposited onto these imprinted nanofibers were found to provide approximately 50% lower enhancement factors than those of the cicada wings themselves. Since silver coatings are prone to forming prohibitively thick oxide layers over time, the production of these substrates on an industrial scale would require a more chemically inert and biocompatible coating, such as gold. Gold is known to produce lower SERS enhancement factors than silver, sometimes by as much as a factor of 10^2 [30] and hence would reduce the imprinted nanofibers' enhancement factors significantly.

Another recently developed naturally inspired silver-coated SERS substrate employed the use of algae diatomic microshell monolayers which yielded maximum enhancement factors of 10^6 [31]. The substrates produced in this method were not macroscopically homogeneous, instead exhibiting a large degree of structural variability across the substrate which could prove to provide inconsistent SERS spectra. A variety of production methods for macroscopically homogeneous two-dimensional SERS substrates have been developed, including chemical etching,

electron-beam lithography, chemical etching, colloid immobilization, annealing of metal ion-implanted silicon, and nanosphere lithography [32–35]. The substrates produced using these techniques provide reproducible SERS enhancement factors of the order of 10^5–10^7. Unfortunately, these production methods are generally prohibitively expensive, complex, and ultimately unsuitable to mass production. Since the substrates' nanostructures are too delicate to withstand cleaning, they are only suitable for single use. For these reasons, cheaper, faster, and more reproducible manufacturing processes are required. This chapter discusses the research undertaken which attempts to address this issue by identifying and reproducing naturally occurring nanostructures for use in SERS.

4 Experimental and Instrumental Methodology

4.1 Preparation and Characterization of SERS Substrates

Since there is such a wide variety of naturally occurring nanostructures with different sizes, spacing, and periodicities of the surface features, it is to be expected that not all will be suitable for SERS. Therefore, when selecting candidate structures for further investigation, one is posed with the question of how to determine which are most suitable. Some naturally occurring nanostructured surfaces have been found to exhibit color changes after being coated with gold, as a result of localized surface plasmon resonances (LSPRs) causing selective photon absorption [36]. Given that LSPRs are a major contributing factor to the SERS effect, it is perhaps reasonable to select and compare potential nanostructured SERS candidate materials on the basis of such color changes after metal deposition. The nanostructured surfaces may also be compared with the shape, spacing, and pitch of structures on well-established SERS substrates using electron microscopy. However, these methods are not always sufficient to determine which nanostructured surface will provide the most effective SERS substrate. For this, a quantitative approach must be taken.

In order to determine the efficacy of a SERS substrate for a given adsorbed molecule, it is necessary to quantify the degree to which the substrate increases the Raman scattered signal with respect to the non-SERS Raman scattered signal of the same molecule. This "enhancement factor" (EF) is most usually defined as:

$$\mathrm{EF} = \frac{I_{\mathrm{SERS}}/N_{\mathrm{Surf}}}{I_{\mathrm{RS}}/N_{\mathrm{Vol}}},$$

where N_{Vol} and N_{Surf} are the average number of molecules within the focal volume for the non-SERS Raman measurement, and the average number of adsorbed molecules on the SERS substrate within the focal volume, respectively [37]. The value for EF is therefore obtained by determining the average enhanced Raman signal intensity per molecule adsorbed to the substrate surface and dividing this value by the average signal obtained per molecule in bulk solution or solid.

A variety of molecules have been used for determining the enhancement factors of SERS substrates, including Rhodamine 6, crystal violet, and thiophenol. The choice of molecule in this task is nontrivial since resonance and "pre-resonance" effects may artificially skew the calculated EF, especially for dye molecules. Although the Raman cross sections for dye molecules are known to be larger than those for smaller molecules by up to 10^6 times, it is often not appreciated that pre-resonance effects mean these dyes may still exhibit large Raman cross sections even under nonresonance conditions [37]. Enhancements from pre-resonance effects can contribute as much as $10\times$ to the EF when the excitation laser used is up to as much as several hundred wavenumbers below the molecule's electronic transition wavelength. The pre-resonance effect has been shown to lead to calculated EFs that are several orders of magnitude greater when dye molecules are used in preference to smaller molecules. These findings prompted the postulation that the highest reported calculated SERS enhancement factors may, in fact, have been several orders of magnitude larger than they would have been if smaller molecules had been used.

Thiophenol, also known as benzene thiol, is a small molecule that does not exhibit the pre-resonance issues of dye molecules. Thiophenol has been shown to produce relatively stable monolayers on silver and gold surfaces which make it a convenient reference compound for SERS substrates [28, 29, 38, 39]. When the SERS substrate is immersed in an ethanolic solution of thiophenol, the sulfur groups form covalent bonds with the metal surface, forming self-assembled monolayers over time, as illustrated in Fig. 4.1.

The standard preparation technique for these monolayers in SERS experiments is immersion of the substrate for 10 min in a 10 mM ethanolic solution of thiophenol [28, 29, 40]. The resulting enhanced Raman spectra obtained from the thiophenol monolayers exhibit well-characterized peaks as shown by Garrett et al. in Fig. 4.2 [40]. For the SERS spectra of the thiophenol monolayers shown in Fig. 4.2, Garrett et al. gave peak assignments of the most prominent Raman bands based on those given in previous work [41, 42] as follows; 1,574 cm^{-1} (C–C stretching); 1,072 cm^{-1} (in plane C–C–C stretch and C–S stretching); 1,022 cm^{-1} (out of plane C–H stretching); 999 cm^{-1} (out-of-plane C–C–C stretch); 630 cm^{-1} (out-of-plane C–C–C and C–S stretching) [40].

Enhancement factors of naturally occurring nanostructures typically range from 10^6 for gold-coated structures, such as cicada and butterfly wings, and 10^7 for silver-coated structures [28, 40]. The choice of metal is very important when producing SERS substrates. Silver is expected to give a greater SERS enhancement than gold due to the greater participation of interband transitions in silver's dielectric function. However, since silver oxidizes rapidly, SERS substrates coated with silver have a short shelf life compared with those coated in gold. Additionally, silver may react with molecules being investigated with SERS. For these reasons, gold is often preferred to silver, especially for applications where the substrate needs to be inert, in spite of the lower enhancement factors achieved.

To prepare naturally occurring nanostructures for SERS, the samples must be sectioned, cleaned, mounted onto a suitable medium (such as a glass substrate), and

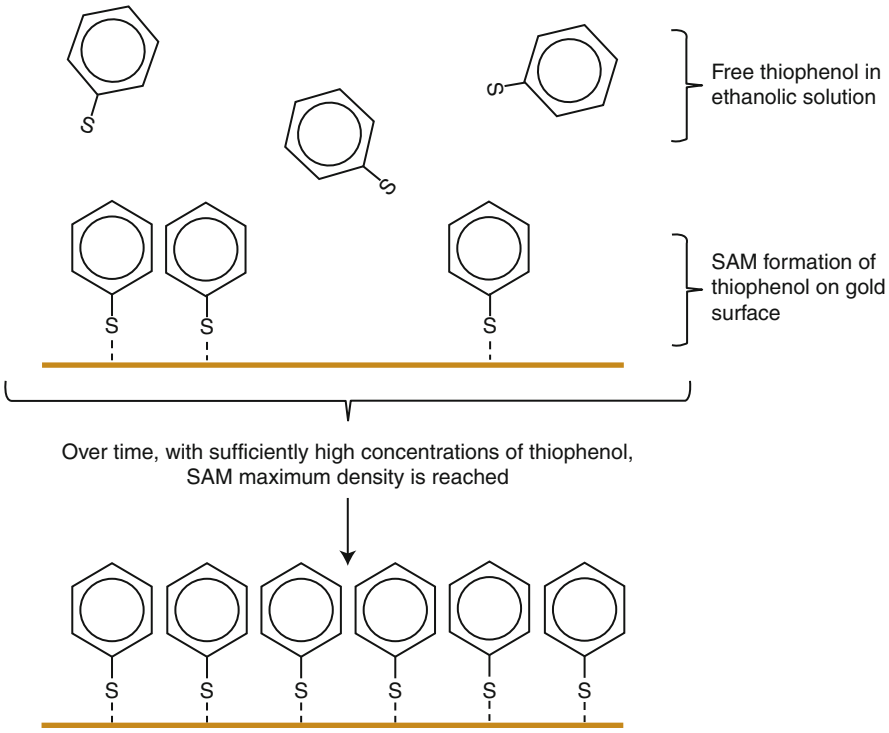

Fig. 4.1 Schematic diagram illustrating the formation of a self-assembled monolayer (SAM) of thiophenol on a gold surface

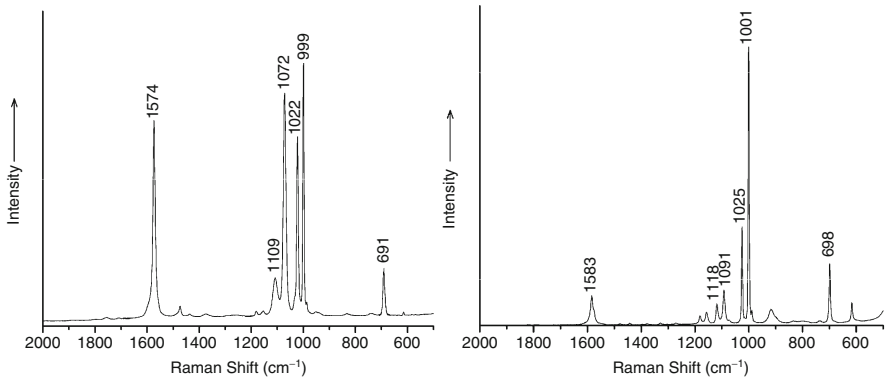

Fig. 4.2 SERS spectra of a thiophenol monolayer on a butterfly wing coated with 70 nm silver (*left*) and an un-enhanced Raman spectrum of neat thiophenol in solution (*right*), with permission from [40]

coated with the metal of choice. The method of sectioning and mounting is nontrivial and the choice of mounting method will depend on the intended experimental procedure. For example, when affixing sections of *Graphium weiskei* wings to ultraclean glass microscope slides SERS substrates, Garrett et al. used an optical adhesive (Norland Optical Adhesive, Cranbury, USA) that cured under ultraviolet light [40]. This adhesive formed a strong bond with the glass that was able to withstand immersion in acidic solutions for hours at a time, as well as maintaining its integrity during metal deposition under vacuum. Some of the most reliable methods for coating substrates with metal in a controllable fashion are physical vapor deposition techniques such as sputter coating and thermal evaporation. In these processes, metal is deposited on a surface at a controlled rate (often monitored using a quartz crystal microbalance), first forming island films, and gradually producing continuous layers of metal as the deposited thickness increases. Once coated in metal, the samples may then be characterized using electron microscopy and by using a characterization compound such as thiophenol to determine the SERS enhancement factors.

One of the main purposes of identifying naturally occurring nanostructures for use in SERS is to produce novel substrates. Many methods have been used to manufacture nanostructures for SERS substrates, including electron beam lithography, chemical etching, colloid immobilization, annealing of metal ion-implanted silicon, and nanosphere lithography [32–35]. As explained earlier, although these methods provide reproducible substrates with high enhancement factors, they are time consuming and often prohibitively cost inefficient for single-use substrates. Therefore, alternative manufacturing processes have been investigated to produce copies of nanostructures found in nature for use in SERS. The work undertaken to investigate naturally occurring nanostructures on butterfly wings by Garrett et al. and cicada wings by Stoddart and Kostovski et al. for SERS will now be described, together with their techniques for replicating the nanostructures.

4.2 Butterfly Wings as SERS Substrates for Protein-Binding Assaying

Butterfly wings have long been known to exhibit nanostructured surfaces composed of a structural protein, chitin [21, 43, 44]. These structures give rise to a wide range of startling optical effects such as vivid coloration and iridescence. The *G. weiskei* butterfly investigated for use as a SERS substrate is shown in Fig. 4.3 [40]. SEM images of the dorsal side of the wings shown in Fig. 4.4 indicated that the blue, purple, and pink regions (marked A – F on Fig. 4.3) exhibited conical nanostructures innervated with hair-like scales, which were similar to the *Sensilla trichodea* found on a different variety of *Graphium* butterfly reported elsewhere [45]. The conical nanostructures, shown in Fig. 4.4, were typically found to be ~2 μm in height and ~1 μm in diameter at their widest point.

In contrast to the brightly colored regions of the butterfly wings, the brown areas were found to be covered by shield-shaped scales as shown in Fig. 4.5, which were

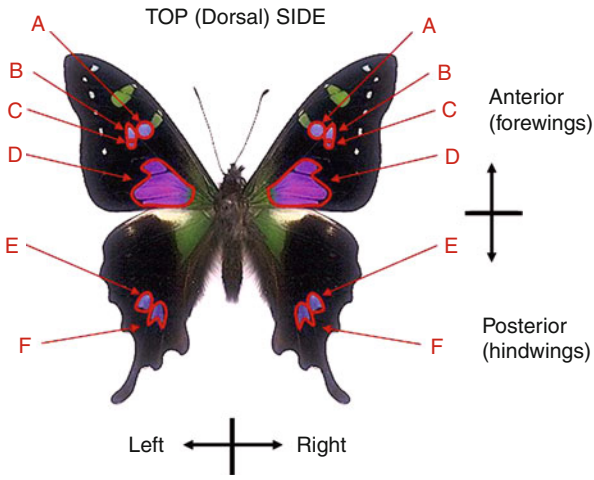

Fig. 4.3 Regions of interest on *G. weiskei* butterfly wings

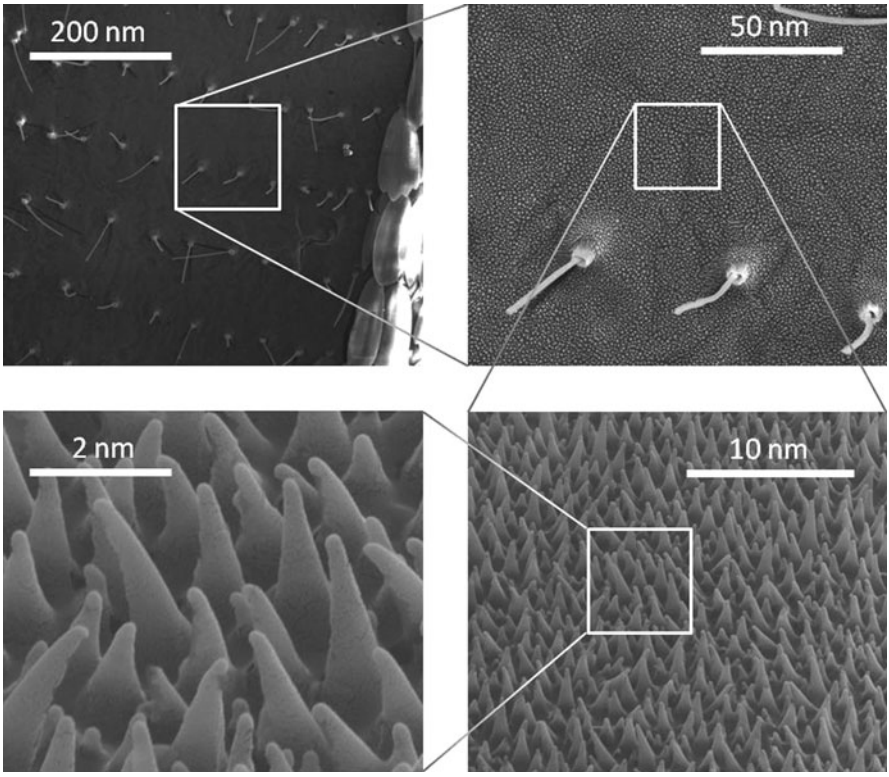

Fig. 4.4 SEM images of the brightly colored regions of *G. weiskei* typically found in regions *A–F* of Fig. 4.3, illustrating the macroscopic hair-like scales (*Sensilla trichodea*) that are characteristic of these regions and the quasi-periodic nanocone structures found between them (Reproduced with permission from [40])

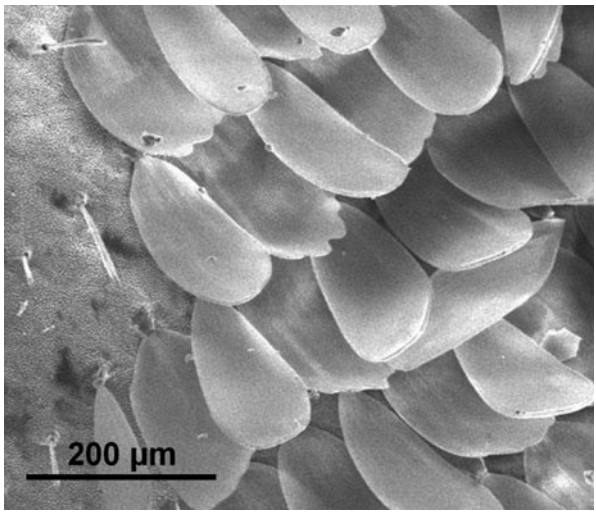

Fig. 4.5 SEM image of the shield-shaped scales covering the brown regions on *G. weiskei*

approximately ~200 nm in length and ~80 nm in width. These regions did not exhibit any nanoscale features suitable for use in SERS, and so were disregarded for the remainder of the study.

To demonstrate the application of these butterfly wing SERS substrates to the problem of protein-binding detection, Garrett et al. devised a protein-binding assay. There are a variety of methods for binding proteins to a metal surface, some of which depend on the amino acid composition of the protein, others of which do not. Direct adsorption via covalent bonds between sulfur groups in proteins and metal surfaces has been used with some success [43]; however, this method is unsuitable for use in Raman spectroscopy-based assays, as nonspecific binding may result in a wide variety of conformational orientations of the molecules with respect to the metal's surface. This can lead to Raman spectra that are difficult to reproduce. Not only that, but the analyte may bind to the metal as well as the antibody, which can lead to noisy spectra.

Other methods of protein binding to metals involve the formation of self-assembled monolayers (SAMs) of linker molecules. Self-assembled monolayers of linker molecules can be straightforward to produce [44, 45] and enable a greater degree of specificity for antibody binding, both in terms of molecular conformation on the SAM surface and in terms of which protein is bound. The model immunoassay was performed by conjugating avidin onto the metalized wing surfaces and using the SERS spectra to detect biotin binding as a function of biotin concentration. The linker molecule 3-mercaptopropanoic acid (MPA) forms covalent bonds with metals via the terminal sulfur groups and can be conjugated to proteins via their NH_2/COOH groups using carbodiimide coupling. When forming monolayers, the MPA molecules can orient themselves in different conformations with respect to the first carbon atom (that which is bound to the sulfur atom). These conformations are termed *gauche* and *trans* configurations, as shown schematically in Fig. 4.2.

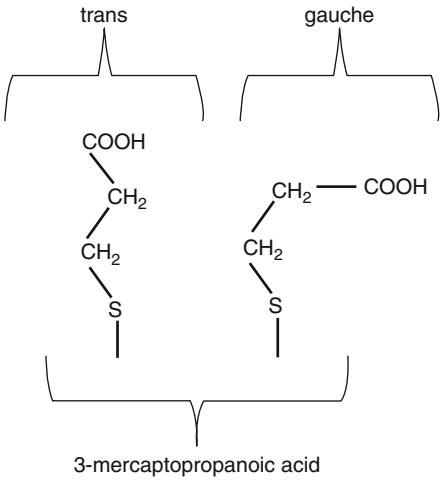

Fig. 4.6 A schematic diagram depicting the chemical conformation of *gauche* and *trans* configurations of 3-mercaptopropanoic acid

The ratio of *gauche* to *trans* configurations in the monolayers is affected by a number of factors including pH, concentration of the molecule in solution, the time over which the SAM is allowed to form, and properties of the metal surface [46].

Immediately after immersion in a solution of MPA, the monolayer packing density on the metal surface is low and the *trans* conformation predominates. Over time, as more molecules adsorb to the metal surface, the *gauche* conformation becomes more common. With silver, the metal surface has a tendency to oxidize in aqueous environments which results in desorption of molecules from the monolayer over time; thus the molecular orientation tends toward the *trans* configuration (Fig. 4.6).

The ratio of *gauche* to *trans* configured molecules may be determined by examining the Raman spectrum. For MPA, the 654 cm^{-1} band is characteristic for a *gauche* S-C-C chain and the 735 cm^{-1} band is characteristic for a *trans* conformer [48–50]. The relative peak heights for the *gauche* and *trans* Raman peaks gives an indication of the relative proportions of the number of molecules in these orientations. In the *gauche* conformation, the terminal binding groups of MPA are less able to bind with proteins during conjugation, so a monolayer of binding molecules in the *trans* conformation is preferable. In order to determine the optimum deposition time for MPA, a time study of the *gauche*: *trans* peak heights was undertaken.

In order to functionalize the metal-coated substrates with MPA, they were immersed in an ethanolic solution of 0.02 M MPA. The MPA layer was activated using a solution of 0.002 M ethyl dimethylaminopropyl carbodiimide (EDC) and 0.005 M n-hydroxy succinimide (NHS) in 2-(*N*-morpholino) ethanesulfonic acid (MES) buffer solution (20 mM MES, 0.1 M NaCl, pH5). The carboxylate groups of the MPA react with NHS in the presence of EDC to form NHS-esters which can then react with amine groups of proteins. After 15 min of activation, the metalized

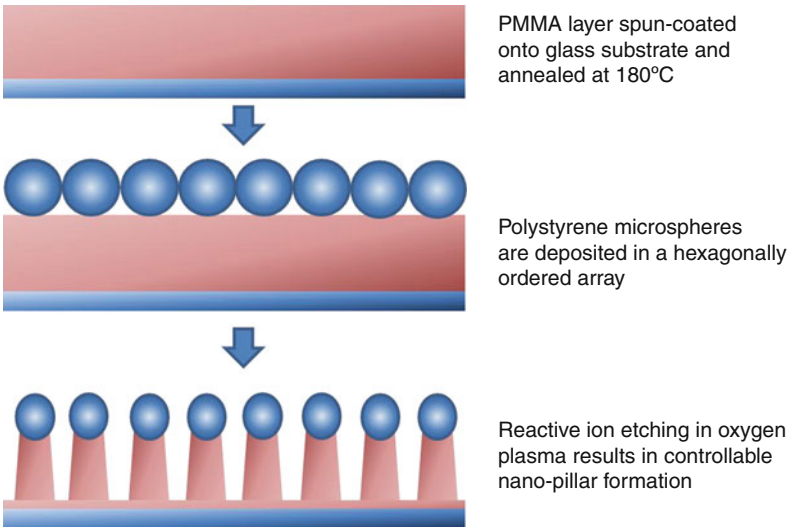

Fig. 4.7 Schematic diagram depicting the reactive ion etching (RIE) technique used to produce arrays of nanoscale pillars of polymer on a glass substrate

samples were rinsed in phosphate buffered saline (PBS) at pH 7. 50 μL aliquots of avidin solution (Sigma Aldrich) at 10 mg/mL in PBS at pH 7 were deposited onto each silvered wing section, and left to incubate for 30 min at 4°C. After incubation, the samples were rinsed in PBS pH 7 and immersed in a quenching solution of 1 M ethanolamine in PBS for 30 min at 4°C to deactivate any unreacted NHS-esters. Following immersion in the quenching solution, the silvered samples were rinsed in PBS pH 7. Aliquots of biotin solutions over a range of concentrations were then added and allowed to bind for 20 min at 4°C. The samples were then rinsed in Millipore water (PURITE, Oxford, UK) and the active area kept hydrated under a droplet of PBS to prevent the proteins from denaturing.

Normal (un-enhanced) Raman spectra of biotin and avidin were obtained using the following procedure. Aqueous solutions at working concentrations of the various chemicals used throughout these experiments were deposited onto aluminum-coated glass microscope slides. Once these drops had dried sufficiently to produce the characteristic "coffee ring" shaped deposition, normal Raman spectra were acquired for comparison with the SERS spectra.

The nanoconical arrays found on the butterfly wings were replicated using a reactive ion etching (RIE) technique illustrated schematically in Fig. 4.7, which was first devised by Weekes et al. [46]. Briefly, glass substrates were spin-coated with a 1.5 μm thick layer of PMMA, which was then annealed at 180°C. Nanostructured arrays were produced by forming hexagonally ordered monolayers of 390 nm diameter polystyrene microspheres upon the PMMA, which were then used as masks for reactive-ion etching (RIE). Reactive ion etching was applied for 8 min in oxygen plasma produced by a 15 W RF source at a base pressure of oxygen at 50 mTorr.

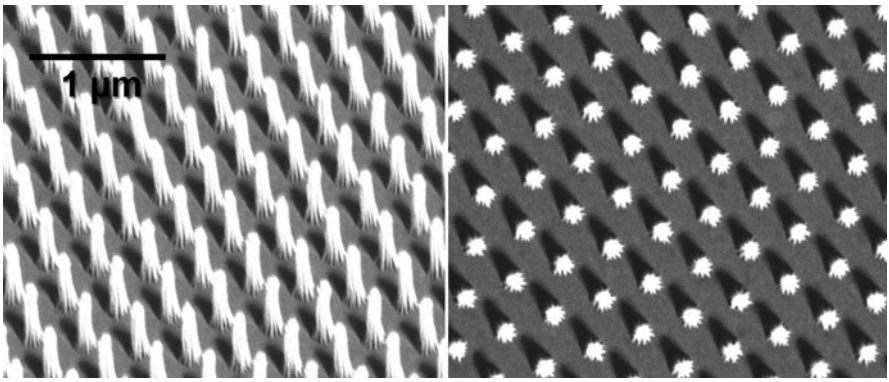

Fig. 4.8 SEM images of the biomimetic nanopillar substrate with pillar heights of 524 nm peak-to-peak distances of 390 nm

The RIE samples produced using this technique were formed over areas of ~1 cm^2. These samples could easily be broken up to create dozens of samples ready for batch-coating with metal, thus providing an efficient means of substrate production. Their SERS enhancement factors were determined in the same manner as for the butterfly wing substrates, and were found to be of similar magnitude.

The RIE biomimetic wing substrates were coated with silver and gold, and investigated in the same manner as the butterfly wings. When imaged using SEM, as shown in Fig. 4.8, they were found to exhibit highly ordered and regular, reproducible arrays of nanopillars.

4.3 Cicada Wings for SERS and a Simple Lithographic Technique for Replicating Their Nanostructure

The optical effects of the quasi-periodic tapered papillary structures found on the surfaces of cicada wings were initially investigated by Stoddart et al. [28]. As illustrated in Fig. 4.9, using scanning electron microscopy, they found that the pattern generated by these nanostructures on the wing surface was generally hexagonal within domains of between 1 and 2 μm^2. Unlike the *G. weiskei* butterfly, this structural morphology was found to be the same in the cicadas irrespective of gender, and was identical on both the upper and lower surfaces of the wings.

Sections of wing samples from *Cicadetta celis* cicadas were coated in a layer of high purity (99.99%) silver 60 nm thick using a Kurt J Lesker CMS-18HV electron beam deposition system controlled by a quartz crystal microbalance. These cicada wing substrates were found to produce a SERS enhancement factor of 10^6 when self-assembled monolayers of thiophenol were formed on their metalized surfaces. More recent work by Kostovski et al. has focused on

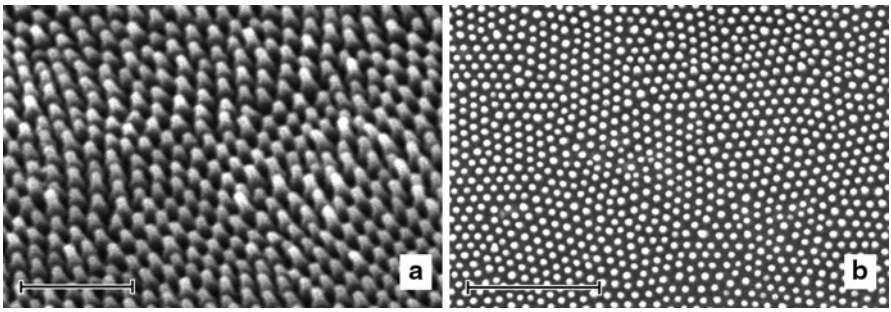

Fig. 4.9 SEM images to illustrate the nanostructures on gold-coated *C. celis* cicada wings taken (**a**) at an angle to the surface of the wing, and (**b**) from a direction normal to the upper surface. Scale bars are 1 μm and 2 μm in (**a**) and (**b**) respectively (Reproduced with permission from [28])

trying to replicate these cicada wing nanostructures for high throughput, high precision, and cost-effective SERS substrate production [29, 47].

The techniques employed by Kostovski et al. have involved nanoimprint ligthography, initially using a relatively labor-intensive technique illustrated in Fig. 4.10. In this method, moulds were made of 9 mm^2 sections of *Cyclochila australasiae* cicada wing by drip coating them with an elastomer solution (h-PDMS). Filling of the nanostructure with the elastomer was encouraged by degassing the sample under vacuum for 10 min, after which time the wing was placed coated side down onto a glass wafer.

The elastomer was cured by heating at 60°C for 12 h before the structure was pried off the wing manually with a scalpel blade. Once formed, these moulds were used to imprint nanostructures onto polymer coatings attached to the end of optical fibers, which was cured using a combination of heating and exposure to ultraviolet light. Finally, the optical fiber tips were coated in silver deposited at an angle of 60° to the fiber's long axis. The cicada wings, nanostructures, and optical fibers are illustrated in Fig. 4.11.

Although effective, this nano imprint lithography technique produced substrates with slightly lower SERS enhancements than those provided by the wings themselves. Additionally, the multistage method described is time consuming and labor intensive. However, Kostovski et al. recently improved upon this technique using a more rapid method for imprinting arrays of optical fibers, as illustrated in Fig. 4.12.

The optical fibers were loaded in an array of up to 40 fibers each placed in an individual U-shaped groove cut into an aluminum block, shown in Fig. 4.13. This technique allowed multiple fibers to be imprinted with the cicada wing mould in a simple and rapid manner that was not critically reliant upon alignment. The resolution obtained with this method was better than 15 nm, producing bidirectional optical fiber prober for SERS with enhancement factors only slightly less than those obtained from the original structures on the cicada wings.

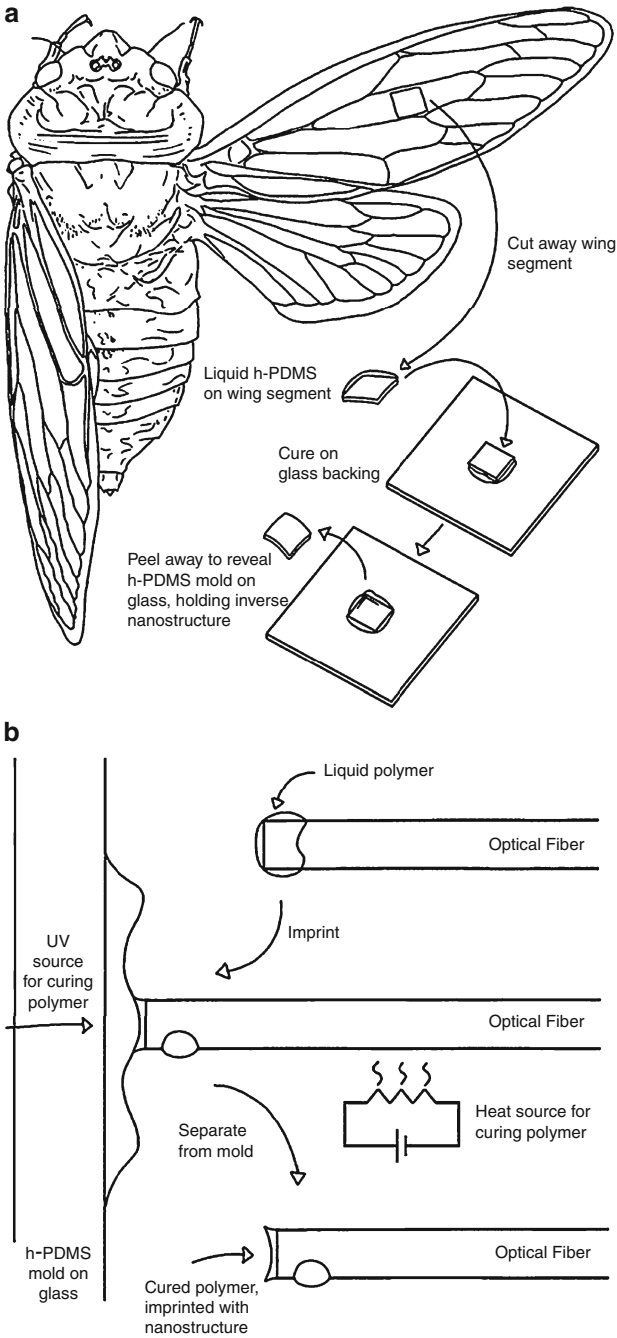

Fig. 4.10 Schematic process diagram illustrating the method used by Kostovski et al. to reproduce the nanostructures found on cicada wings, reproduced with permission [29]

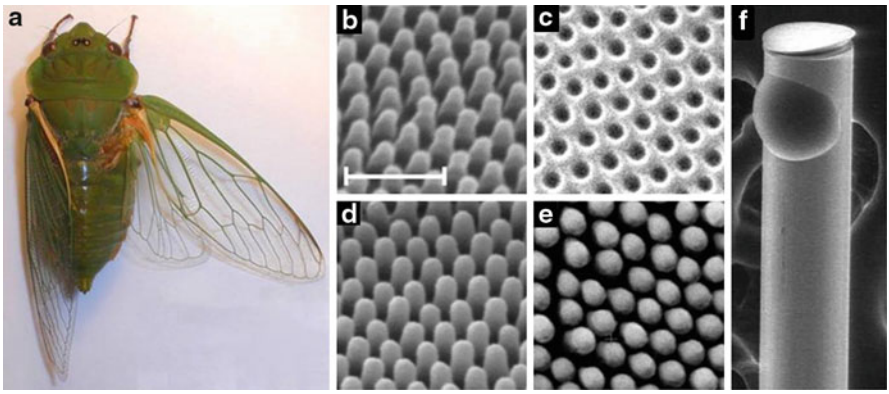

Fig. 4.11 (**a**) A photograph of the Australian greengrocer cicada. SEM images of (**b**) the nanotemplate of the cicada wing nanostructures (the scale bar is 500 nm), (**c**) the inverse h-PDMS mould, (**d**) an optical fiber exhibiting the polymer nanostructure replica, (**e**) the replica coated in silver, and (**f**) a macroscopic image of the imprinted fiber (Reproduced with permission from [29])

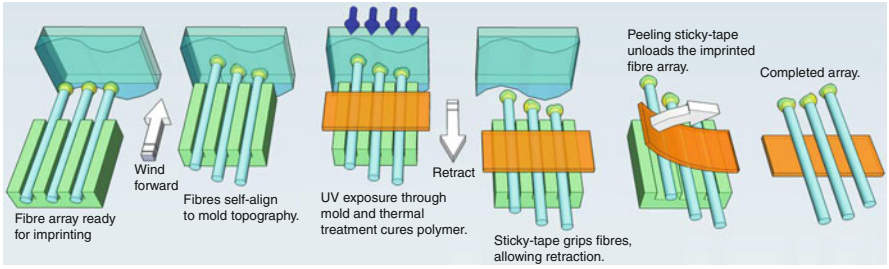

Fig. 4.12 A process schematic diagram of the rapid, self-aligned array-imprinting sequence used by Kostovski et al. to reproduce nanostructures on optical fibers using a nonplanar mould (Reproduced with permission from [47])

5 Key Research Findings

To determine the enhancement factors of *G. weiskei* wings and the biomimetic analogs made using reactive ion etching, Garrett et al. estimated the number of Raman counts per molecule in the SERS spectrum of the substrates by assuming that the thiophenol monolayer was at maximum density [40]. The maximum coverage of alkanethiols on thermally evaporated gold substrates has been shown to be 21%; 2.5×10^{14} molecules/cm^2 $\pm 0.1 \times 10^{14}$ molecules [48]. Assuming maximum metal coverage, this provides a conservative estimate for the enhancement factor, since maximum density monolayers of alkanethiols typically take 1–2 h to form, whereas SERS substrates have typically been characterized using SAMs of thiophenol formed over 10 min [49], hence in order to be able to compare the substrates investigated in this study with others reported elsewhere, it was necessary

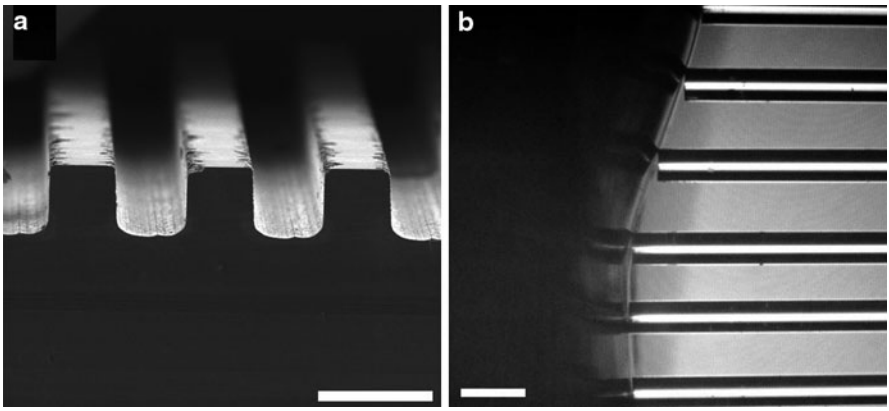

Fig. 4.13 SEM image of the diced "U-grooves" (**a**), and a photograph of the fiber-array (**b**) self-aligning against a nonplanar mould, as used by Kostovski et al. (Reproduced with permission from [47])

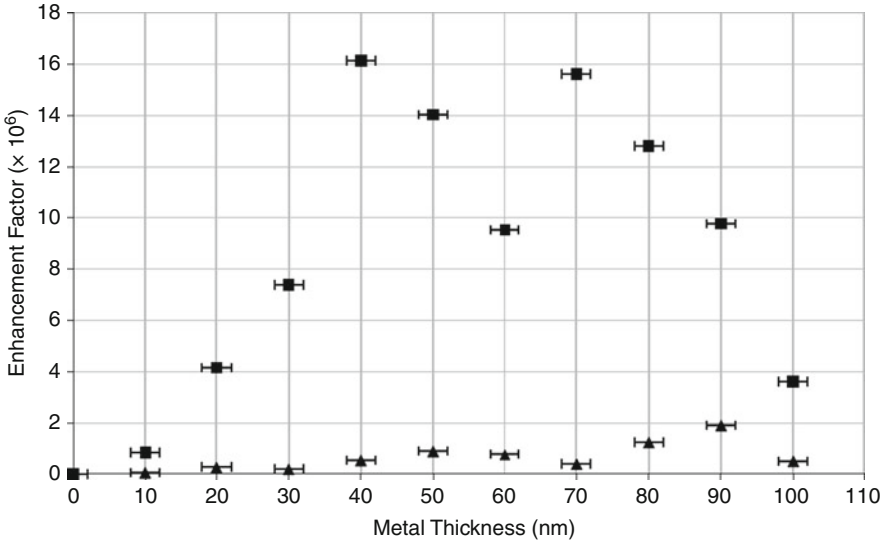

Fig. 4.14 Enhancement factor of metalized wing nanostructures as a function of metal deposition thickness: ■ data points correspond with silver, ▲ with gold

to use this reduced SAM formation time. The area of the substrate illuminated by the objective was calculated from the Airy disc diameter; hence the number of thiophenol molecules in the focal area was estimated at $6.0 \times 10^6 \pm 1.3 \times 10^4$.

A range of metal thicknesses was explored, in order to determine the optimum deposition thickness. Average enhancements over three wing sections and thirty scans were taken for each data point, the standard errors of which were too small to

depict on the graph in Fig. 4.14. The enhancement factor depends on a combination of the metal thickness over each nanocone, the geometric feature sharpness (both at the tips of the nanocones and at the cavities at their bases), and the nanocone spacing. Therefore, as the deposited metal thickness increases, these features will be changed, causing both the intensity and resonant wavelength of the surface plasmons to be altered, which has led to the graph shape shown in Fig. 4.14. The difference in peak thickness and intensity for gold and silver arises from their differing dielectric constants.

When corrected for acquisition times, the maximum enhancement factors for the metalized *G. weiskei* wing surfaces were found to be $1.9 \times 10^6 \pm 5.8 \times 10^4$ for gold, and $1.6 \times 10^7 \pm 1.8 \times 10^5$ for silver. For the biomimetic substrates, the maximum enhancement factors were $1.1 \times 10^6 \pm 5.1 \times 10^4$ for gold and $1.4 \times 10^7 \pm 1.7 \times 10^5$ for silver [40].

The MPA molecule binds to metal surfaces via a covalent bond from the sulfur group. If the concentration of MPA molecules on a metal surface is high, the molecules tend to orient themselves in a *trans* configuration, whereas if the concentration is low, the MPA molecules will have a higher instance of *gauche* configuration. In the *gauche* configuration, the protein-binding site of the MPA molecule is less accessible than those in the *trans* configuration; the optimal MPA deposition time was determined by performing depositions for a range of times and comparing the ratios of the *gauche* and *trans* peaks (at 654 and 735 cm^{-1}, respectively) [50–52]. After immersing metalized wing substrates in ethanolic solutions of MPA for a range of times up to 18 h, the optimal deposition time was determined as 2 h. Upon activation of the MPA monolayer, the carboxyl band at 900 cm^{-1} shifted to 928 cm^{-1}, indicating that the carboxyl group was dissociated (Fig. 4.15).

Once avidin molecules were bound to an MPA monolayer, SERS spectra were acquired (see Fig. 4.16). The most prominent peaks in the hydrated avidin SERS spectrum were tentatively assigned to phenylalanine (1,001 cm^{-1}, 1,030 cm^{-1}), tryptophan (759 cm^{-1}, 875 cm^{-1}, 930 cm^{-1}, 960 cm^{-1}, 1,001 cm^{-1}, 1,357 cm^{-1}, 1,546 cm^{-1}, and 1,580 cm^{-1}), tyrosine (827 cm^{-1}, 852 cm^{-1}), C–C stretching (930 cm^{-1}), COO symmetric stretching (1,400 cm^{-1}). These peak assignments corresponded well with the spontaneous Raman spectrum of avidin (see Fig. 4.17). The amide I and amide III regions were located at 1,665 and 1,237 cm^{-1}, respectively. Each avidin peak lay within 6 cm^{-1} of the same peak assignments for the lyophilized avidin spectrum reported by Fagnano et al. [53]. A 6 cm^{-1} discrepancy is reasonable given the conformational changes that can occur between hydrated and lyophilized proteins, combined with the 2–3 cm^{-1} limit of resolution of the system.

It was found that upon binding to biotin, the intensity of the 960 cm^{-1} tryptophan peak increased relative to the 1,001 cm^{-1} phenylalanine peak (see Fig. 4.17), as reported by Fagnano et al. [53]. Since the avidin-binding site contains the amino acids phenylalanine, alanine, asparagine, and tryptophan [54], the 960 cm^{-1} tryptophan peak and the 1,001 cm^{-1} phenylalanine peak were chosen as binding indicator peaks for investigation in the SERS assay. The amide I and amide III bands did not change significantly upon addition of biotin.

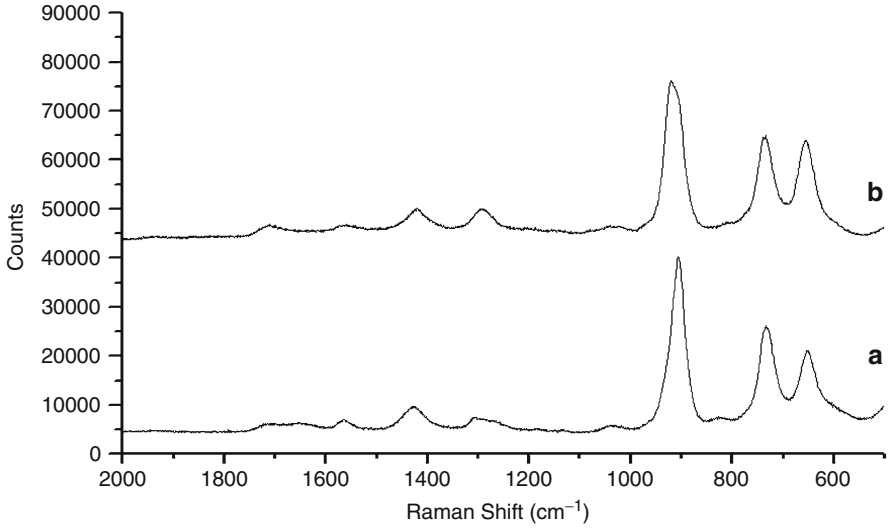

Fig. 4.15 SERS spectra of MPA (**a**) prior to activation with EDC/NHS, (**b**) after activation (Reproduced with permission from [40])

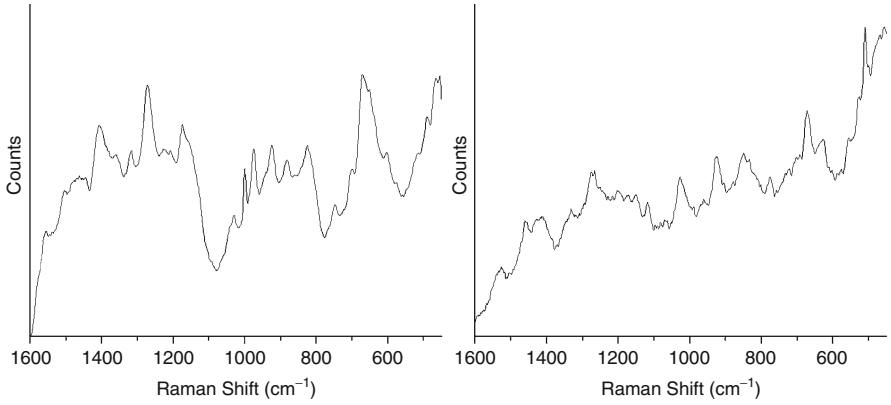

Fig. 4.16 SERS spectra of avidin bound to gold-coated wing (*right*) and the avidin-biotin complex bound to gold-coated wing (*left*) (Reproduced with permission from [40])

Upon addition of biotin, two distinct peaks were found in the avidin-biotin complex spectra which were indicative of the complex formation, 975 and 1,000 cm^{-1}, which were attributed to the avidin-binding site amino acids phenylalanine, alanine, asparagine, and tryptophan [54, 55]. It was found that the 1,000 cm^{-1} peak decreased in strength relative to the 975 cm^{-1} peak with increasing biotin concentration as shown in Fig. 4.19; an attribute exploited to perform a biotin assay. When plotted on a log scale as shown in Fig. 4.18, the assay gave a log-linear response over a range of 0.5–1,000 nM (equivalent to 0.12 ng/mL–0.24 μg/mL)

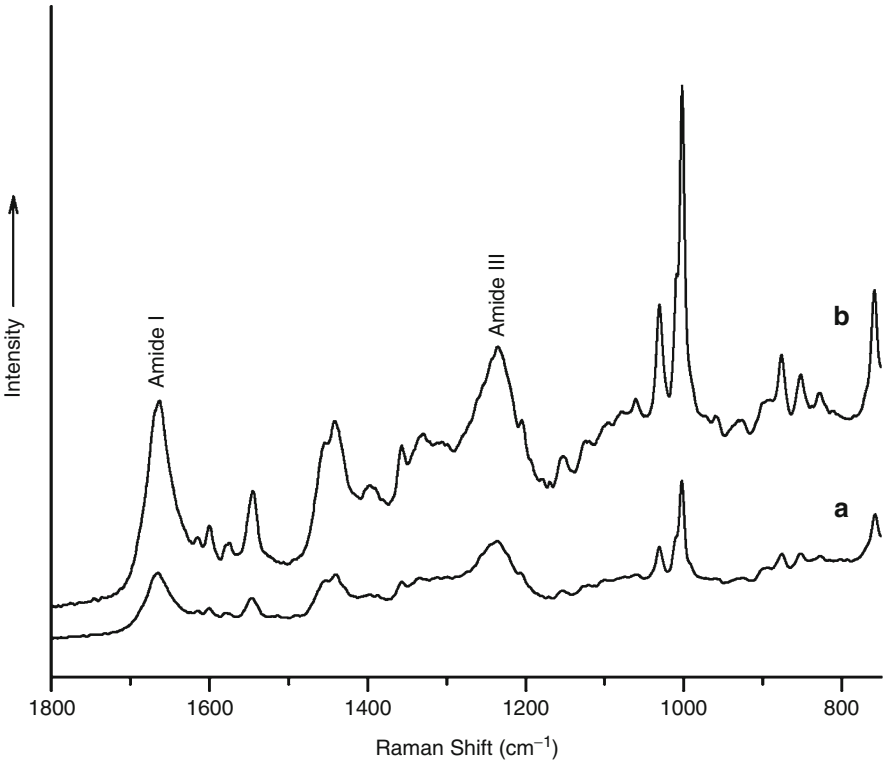

Fig. 4.17 Normal Raman spectra for avidin (**a**) and avidin-biotin (**b**) (Reproduced with permission from [40])

solutions of biotin suspended in buffer solution. The limit of detection of this assay was 0.2 nM (49 pg/mL).

Gold-coated butterfly wing nanostructures can provide excellent SERS substrates for use with protein assaying without the need for dehydrating the sample – a major advantage over other nanostructures surfaces used as SERS substrates. The entire avidin/biotin assay took no more than 4 h from surface conjugation to SERS scanning, which is comparable to some of the more rapid ELISA assays commercially available. The volume of analyte used was very small (only 30 μL), which would be an advantage for applications in areas such as forensics where it is often impractical or impossible to perform assays on large volumes of analyte.

When coated with 90 nm of gold, the substrates produced were found to provide consistent enhancement for up to 2 weeks after evaporation, when stored in a dessicator. Silver-coated substrates generally provided enhancement factors that were only consistent when used within 48 h after evaporation, due to oxide layer formation. In addition, gold is known to be markedly more biologically inert than

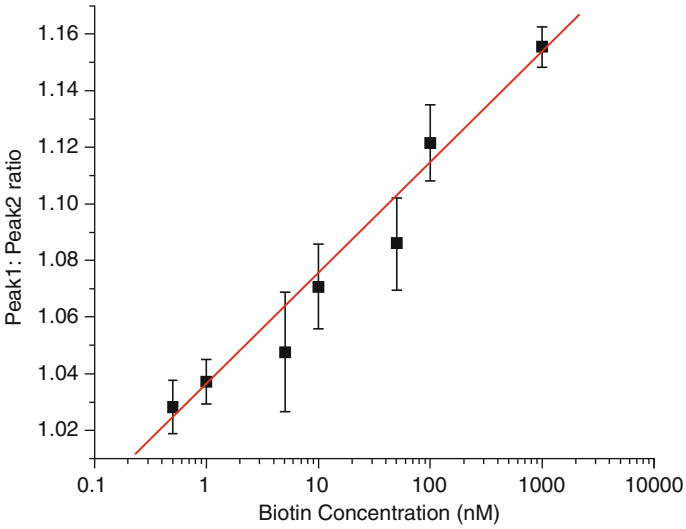

Fig. 4.18 Ratios of the heights of the peaks at 975 cm^{-1} (peak 1) and 1,000 cm^{-1} (peak 2) in the SERS spectra of the avidin-biotin complex for gold-coated butterfly wings for a range of concentrations of biotin in buffer solution (Reproduced with permission from [40])

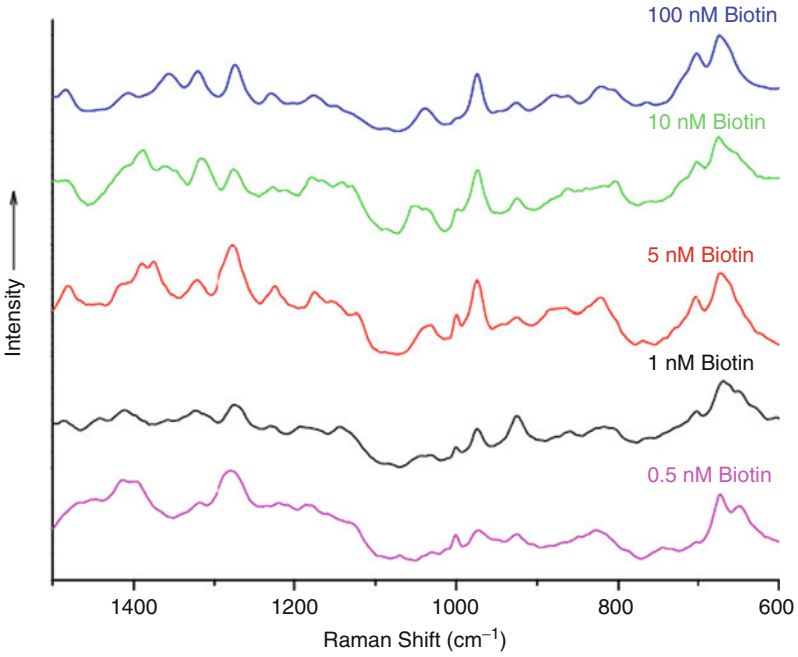

Fig. 4.19 SERS spectra of metalized wing-bound avidin exposed to a range of biotin solution concentrations (Reproduced with permission from [40])

silver, hence gold was preferred for biological applications in spite of the fact that the resulting enhancement factor was ~10× smaller than that obtained with silver.

In order to demonstrate the potential for mimicking the conical nanostructures of the butterfly wings for commercial applications, a simple reactive ion etching technique was employed. The biomimetic substrates showed excellent SERS enhancement factors (1.1×10^6 with a 90 nm coating of gold and 1.4×10^7 for a 70 nm coating of silver), and preliminary biocompatibility experiments showed that these substrates exhibit the remarkable property of enabling SERS signals to be obtained when the scanning area is submerged under a droplet of buffer solution. Future experiments will focus on combining these biomimetic substrate production techniques with nanotransfer printing methods in order to speed up production times and reduce costs, for use with biological applications.

6 Conclusions and Future Perspective

One of the main advantages of the wing-based SERS assay devised by Garrett et al. was the large range of analyte concentrations over which a log-linear response was measured (0.12 ng/mL–0.24 μg/mL) without the need for dilution of the analyte, as illustrated in Fig. 4.18. Until now, SERS assays have been effective over typical analyte concentration ranges spanning only one to two orders or magnitude [3, 4, 7, 8, 14], while ELISA assays have been made with effective concentration ranges of pg/ml to ng/mL [52]. This assay technique has bridged the gap between SERS and ELISA assays, potentially paving the way for commercially viable SERS substrates for undertaking assays of wet biological samples. Since SERS provides detailed structural and chemical information about assay analytes, with effective concentration detection ranges as large as those used in ELISA, SERS could become a much more effective immunoassay choice.

Now that the efficacy of biomimetic substrates for SERS protein assays has been proven, the next stage of research in this field should involve developing a rapid production method of these substrates. The reactive ion etching technique employed to produce the biomimetic substrates in this chapter have yielded highly reproducible nanostructured arrays over areas 1 cm^2 in size after only an 8 min exposure to the oxygen plasma, which could then be broken down to produce up to 25 substrates. Subsequent evaporation of gold took ~2.5 h for up to 12 substrates simultaneously, depending on the thickness of metal required. The total time taken to produce 25 such biomimetic substrates using the techniques outlined above is estimated at 4 h, although for industrial applications this could be greatly improved by adopting a production line technique.

Elastomer templates for nanoimprinting of the type devised by Kostovski et al. for their optical fiber nanoimprint lithography could be used to rapidly reproduce the butterfly wing nanostructures or those produced by reactive ion etching. This would further reduce production time and costs. Whatever means are employed to improve the production techniques for these butterfly and cicada wing substrates, it is clear that there is great potential for their application in biosensing.

References

1. Osawa M (2001) Surface-enhanced infrared absorption. In: Kawata S (ed) Near-field optics and surface plasmon polaritons. Springer, Berlin/Heidelberg, pp 163–187
2. Yonzon CR, Stuart DA, Zhang X et al (2005) Towards advanced chemical and biological nanosensors–an overview. Talanta 67(3):438–448
3. Dou X, Takama T, Yamaguchi Y et al (1997) Enzyme immunoassay utilizing surface-enhanced Raman scattering of the enzyme reaction product. Anal Chem 69(8):1492–1495
4. Moger J, Gribbon P, Sewing A et al (2007) Feasibility study using surface-enhanced Raman spectroscopy for the quantitative detection of tyrosine and serine phosphorylation. Biochim Biophys Acta Gen Subj 1770(6):912–918
5. Xu SP, Ji XH, Xu WQ et al (2005) Surface-enhanced Raman scattering studies on immunoassay. J Biomed Opt 10(3):031112/1–031112/12
6. Dou X, Yamaguchi Y, Yamamoto H et al (1998) NIR SERS detection of immune reaction on gold colloid particles without bound/free antigen separation. J Raman Spectrosc 29(8): 739–742
7. Xu SP, Wang LY, Xu WQ et al (2003) Immunological identification with SERS-labeled immunogold nanoparticles by silver staining. Chem J Chin Univ Chin 24(5):900–902
8. Zhang ML, Yi CQ, Fan X et al (2008) A surface-enhanced Raman spectroscopy substrate for highly sensitive label-free immunoassay. Appl Phys Lett 92(4):043116
9. Levy Y, Onuchic JN (2006) Water mediation in protein folding and molecular recognition. Annu Rev Biophys Biomol Struct 35:389–415
10. Ortiz C, Zhang D, Xie Y et al (2006) Validation of the drop coating deposition Raman method for protein analysis. Anal Biochem 353(2):157–166
11. Ronald A, Stimson WH (1998) The evolution of immunoassay technology. Parasitology 117: S13–S27
12. Hirsch LR, Jackson JB, Lee A et al (2003) A whole blood immunoassay using gold nanoshells. Anal Chem 75(10):2377–2381
13. Ji X, Xu S, Wang L et al (2005) Immunoassay using the probe-labeled Au/Ag core-shell nanoparticles based on surface-enhanced Raman scattering. Colloid Surf A Physicochem Eng Aspects 257–258:171–175
14. Rohr TE, Cotton T, Fan N et al (1989) Immunoassay employing surface-enhanced Raman-spectroscopy. Anal Biochem 182(2):388–398
15. Alexander RM (2005) Book Reviewed: The gecko's foot. Bio-inspiration: engineered from nature (Peter Forbes Hardback book, 272 p, ISBN 0007179901, Class number 620.0042) Nature 438(7065):166–166
16. Kinoshita S, Yoshioka S (2005) Structural colors in biological systems. Osaka University Press, Osaka
17. Parker AR (1999) Inverterbrate structural colour. In: Savazzi E (ed) Functional morphology of the invertebrate skeleton. Wiley, New York
18. Potyrailo RA, Ghiradella H, Vertiatchikh A et al (2007) Morpho butterfly wing scales demonstrate highly selective vapour response. Nat Photonics 1:123–128
19. Srinivasarao M (1999) Nano-optics in the biological world: beetles, butterflies, birds, and moths. Chem Rev 99(7):1935–1961
20. Vukusic P, Sambles JR (2003) Photonic structures in biology. Nature 424(6950):852–855
21. Ghiradella H, Aneshansley D, Eisner T et al (1973) Ultraviolet reflection of a male butterfly: interference color caused by thin-layer elaboration of wing scales. Science 179(4071):415
22. Land MF (1972) The physics and biology of animal reflectors. Prog Biophys Mol Biol 24: 75–106
23. Vukusic P, Wootton RJ, Sambles JR (2004) Remarkable iridescence in the hindwings of the damselfly Neurobasis chinensis chinensis (Linnaeus) (Zygoptera: Calopterygidae). Proc R Soc Lond Ser B Biol Sci 271(1539):595–601

24. Yoshioka S, Kinoshita S (2007) Polarization-sensitive color mixing in the wing of the Madagascan sunset moth. Opt Expr 15(5):2691–2701
25. Volkmer A, Cheng JX, Xie XS (2001) Vibrational imaging with high sensitivity via epidetected coherent anti-stokes Raman scattering microscopy. Phys Rev Lett 8702(2):023901
26. Vukusic P, Hallam B, Noyes J (2007) Brilliant whiteness in ultrathin beetle scales. Science 315(5810):348–351
27. Jewell SA, Vukusic P, Roberts NW (2007) Circularly polarized colour reflection from helicoidal structures in the beetle *Plusiotis boucardi*. New J Phys 9:99
28. Stoddart PR, Cadusch PJ, Boyce TM et al (2006) Optical properties of chitin: surface-enhanced Raman scattering substrates based on antireflection structures on cicada wings. Nanotechnology 17(3):680–686
29. Kostovski G, White DJ, Mitchell A et al (2009) Nanoimprinted optical fibres: biotemplated nanostructures for SERS sensing. Biosens Bioelectron 24(5):1531–1535
30. Kneipp J, Kneipp H, Kneipp K (2008) SERS – a single-molecule and nanoscale tool for bioanalytics. Chem Soc Rev 37:1052–1060
31. Pelletier MJ, Altkorn R (2001) Raman sensitivity enhancement for aqueous protein samples using a liquid-core optical-fiber cell. Anal Chem 73(6):1393–1397
32. Abdelsalam ME, Bartlett PN, Baumberg JJ et al (2005) Electrochemical SERS at a structured gold surface. Electrochem Commun 7(7):740–744
33. Baker GA, Moore DS (2005) Progress in plasmonic engineering of surface-enhanced Raman-scattering substrates toward ultra-trace analysis. Anal Bioanal Chem 382(8):1751–1770
34. Hunyadi SE, Murphy CJ (2006) Bimetallic silver-gold nanowires: fabrication and use in surface-enhanced Raman scattering. J Mater Chem 16(40):3929–3935
35. White DJ, Mazzolini AP, Stoddart PR (2007) Fabrication of a range of SERS substrates on nanostructured multicore optical fibres. J Raman Spectrosc 38(4):377–382
36. Yoshida A, Motoyama M, Kosaku A et al (1997) Antireflective nanoprotuberance array in the transparent wing of a hawkmoth, *Cephonodes hylas*. Zool Sci 14(5):737–741
37. Le Ru EC, Blackie E, Meyer M et al (2007) Surface enhanced Raman scattering enhancement factors: a comprehensive study. J Phys Chem C 111(37):13794–13803
38. Viets C, Hill W (2000) Single-fibre surface-enhanced Raman sensors with angled tips. J Raman Spectrosc 31(7):625–631
39. Haynes CL, McFarland AD, Van Duyne RP (2005) Surface-enhanced Raman spectroscopy. Anal Chem 77(17):338A–346A
40. Garrett NL, Vukusic P, Ogrin F et al (2009) Spectroscopy on the wing: naturally inspired SERS substrates for biochemical analysis. J Biophotonics 2(3):157–166
41. Bryant MA, Pemberton JE (1991) Surface Raman-scattering of self-assembled monolayers formed from 1-alkanethiols at Ag. J Am Chem Soc 113(10):3629–3637
42. Bryant MA, Pemberton JE (1991) Surface Raman-scattering of self-assembled monolayers formed from 1-alkanethiols – behavior of films at Au and comparison to films at Ag. J Am Chem Soc 113(22):8284–8293
43. Brakefield PM, French V (1999) Butterfly wings: the evolution of development of colour patterns. Bioessays 21(5):391–401
44. Vukusic P, Sambles R, Lawrence C et al (2001) Sculpted-multilayer optical effects in two species of Papilio butterfly. Appl Opt 40(7):1116–1125
45. Dey S, Hooroo RNK, Bhattacharjee CR (1998) Electron microscopy and spectroscopical studies on the coloured patches on the wing of a butterfly, *Graphium sarpedon* (Lepidoptera: Papillionidae) with reference to their photobiological and electrical properties. Pigment Cell Res 11(1):1–11
46. Weekes SM, Ogrin FY, Murray WA et al (2007) Macroscopic arrays of magnetic nanostructures from self-assembled nanosphere templates. Langmuir 23(3):1057–1060
47. Kostovski G, Chinnasamy U, Jayawardhana S et al (2011) Sub-15 nm optical fiber nanoimprint lithography: a parallel, self-aligned and portable approach. Adv Mater 23(4):531–535

48. O'Dwyer C, Gay G, Viaria de Lesegno B et al (2005) Advancing atomic nanolithography: cold atomic Cs beam exposure of alkanethiol self assembled monolayers. J Phys Conf Ser 19:109–117
49. Briand E, Salmain M, Henry JM et al (2006) Building of an immunosensor: how can the composition and structure of the thiol attachment layer affect the immunosensor efficiency? Biosens Bioelectron 22(3):440–448
50. Michota A, Kudelski A, Bukowska J (2002) Molecular structure of cysteamine monolayers on silver and gold substrates – comparative studies by surface-enhanced Raman scattering. Surf Sci 502:214–218
51. Kudelski A (2002) Raman study on the structure of 3-mercaptopropionic acid monolayers on silver. Surf Sci 502:219–223
52. Kudelski A, Hill W (1999) Raman study on the structure of cysteamine monolayers on silver. Langmuir 15(9):3162–3168
53. Fagnano C, Fini G, Torreggiani A (1995) Raman spectroscopic study of the avidin-biotin complex. J Raman Spectrosc 26(11):991–995
54. Huang TS, Delange RJ (1971) Egg white avidin. 2. Isolation, composition, and amino acid sequences of tryptic peptides. J Biol Chem 246(3):686
55. Stewart S, Fredericks PM (1999) Surface-enhanced Raman spectroscopy of amino acids adsorbed on an electrochemically prepared silver surface. Spectrochim Acta A Mol Biomol Spectrosc 55(7–8):1641–1660